ORIGINAL RESEARCH

A force field for the solubility of cellulose in DMSO/Ionic liquids

**Eliane Roos · Cora Gradaus ·
Daniel Sebastiani · Martin Brehm**

Abstract We present the extension of our all-atom force field BILFF (*B*io-polymers in *I*onic *L*iquids *F*orce *F*ield) to the co-solvent dimethyl sulfoxide (DMSO). BILFF already includes force field parameters for several imidazolium- and triazolium-based ionic liquids, water, and the bio-molecule cellulose. DMSO is known to increase the cellulose solubility of [EMIm][OAc] when applied as an additive. Our focus is on a correct reproduction of the hydrogen bonds in the ternary system of $[EMIm]^+$, $[OAc]^-$, water and DMSO compared to *ab initio* molecular dynamics simulations. For this purpose, the results from force field MD simulations such as radial and distance–angle distribution functions are compared with the reference AIMD simulation. Based on this, the force field parameters (starting from OPLS–AA) are iteratively adjusted. Four systems, pure and aqueous DMSO as well as DMSO in pure and aqueous [EMIm][OAc], are considered and additionally compared to DMSO-free [EMIm][OAc] systems. A very good agreement with respect to the microstruc-

ture of the quantum chemical reference simulations as well as to experimental data such as density, diffusion coefficients, enthalpy of vaporization, compressibility and thermal expansion coefficients can be observed over a wide temperature range. BILFF thus enables accurate simulations of larger systems of solvated cellulose in (aqueous) [EMIm][OAc] and the co-solvent DMSO.

Keywords DMSO · Force field molecular dynamics simulation · Cellulose Co-solvent · Ionic liquid · Solvent structure · Hydrogen bond lifetime · Calculated volume expansion coefficient · Calculated compressibility

E. Roos · C. Gradaus · D. Sebastiani · M. Brehm (✉)
Institut für Chemie – Theoretische Chemie, Martin-Luther-Universität Halle–Wittenberg, Von-Danckelmann-Platz 4, 06120 Halle (Saale), Germany
Martin_Brehm@gmx.de

M. Brehm
Department Chemie, Universität Paderborn, Warburger Straße 100, 33098 Paderborn, Germany

Introduction

Cellulose is recognized as a nearly limitless resource to fulfill the growing need for environmentally friendly and biocompatible products (Azimi et al. 2022, Klemm et al. 2005, Nanda et al. 2022, Payne et al. 2015). It has diverse applications, spanning from packaging materials and writing surfaces to biofuels (Himmel et al. 2007), bioplastics (Fang et al. 2023), anti fungal membranes (Wanichapichart et al. 2012), laminates (Yousefi Shivyari et al. 2016), and phosphorescent materials (Zhang et al. 2022), among other innovative uses (Abeer et al. 2014, Sun and Cheng 2002, Thomas et al. 2018). Some processes require the dissolution of cellulose. However, the solubility of cel-

lulose in conventional solvents is a challenge due to its extensive inter- and intramolecular hydrogen bonding. Industrially used derivatizing solvents such as carbon disulfide (CS_2) or *N*-methylmorpholine *N*-oxide (NMMO) have several disadvantages such as toxicity, insufficient solvent stability, degradation of both cellulose and solvent and significant stabilizer requirements (Azimi et al. 2022, Olsson and Westman 2013). A direct dissolution of raw cellulose not only simplifies the processing but also circumvents byproduct generation. Therefore, there is a strong interest in discovering environmentally friendly and non-toxic solvents capable of dissolving cellulose without requiring derivatization. In 2002, Swatloski discovered that such a cellulose solvent are ionic liquids (ILs) (Swatloski et al. 2002). A technically relevant cellulose solubility is achieved, for example, in the IL 1-ethyl-3-methylimidazolium acetate ([EMIm][OAc]), which has become the focus of research due to its additional high chemical stability (Froschauer et al. 2013, Le et al. 2012). However, while IL-based methods for processing biomass show promise for large-scale applications, certain ILs can be expensive and have a high viscosity, creating challenges for scaling up (Li et al. 2013). A combination of an IL and polar organic co-solvents, such as dimethyl sulfoxide (DMSO) exhibits a lower viscosity than the pure IL and improves the solubility of cellulose (Anokhina et al. 2017, Mohan et al. 2016, Tomimatsu et al. 2019, Xu et al. 2013, Yang et al. 2019b). However, it is still debated how precisely DMSO enhances the cellulose solubility, while water, also a polar molecule, reduces it: To dissolve cellulose, it is necessary to replace the inter- and intramolecular cellulose hydrogen bonds with solvent–cellulose hydrogen bonds formed primarily by the anion of the IL. However, these interactions are hindered by a strong association between the cation and the anion (Brehm et al. 2019, 2020a). A common theory is that DMSO separates the ions from each other and, by additionally reducing the viscosity and thereby increasing the mass transfer rate (Le et al. 2014), promotes the formation of anion–cellulose hydrogen bonds (Anokhina et al. 2017, Brehm et al. 2019, 2020a, Manna and Ghosh 2019, Mohan et al. 2016, Paiva et al. 2022, Tomimatsu et al. 2019).

Although several studies on cellulose in [EMIm][OAc] and DMSO have been published, the influence of water on the underlying hydrogen bond network has hardly been investigated. However, in view

of the fact that the IL is hygroscopic and that cellulose reprecipitates even in the presence of small amounts of water (Froschauer et al. 2013, Le et al. 2012), the importance of water should not be ignored. To gain a thorough understanding of the intricate interactions present within the cellulose/IL/DMSO/water system at the atomic level, molecular dynamic (MD) simulations can be utilized. However, despite its accuracy, quantum chemical techniques are impractical for studying these large systems due to their high computational demand and time-consuming nature. To overcome these limitations, force fields can be utilized as an empirical alternative for representing the interactions. A force field describes the interactions between molecules in a simplified way by representing the total potential energy as the sum of the contributions from bonds, bond angles, torsion angles, and electrostatic and van der Waals energies. These energy components are parameterized using empirical functions, allowing a force field to focus on specific application fields.

There are already several force field parameter sets available for the molecule DMSO, which have been optimized to accurately describe the thermodynamic properties of pure DMSO and aqueous DMSO (Bordat et al. 2003, Fox and Kollman 1998, Geerke et al. 2004, Strader and Feller 2002). However, there is currently no force field specifically designed to accurately describe the microstructure between an ionic liquid, particularly [EMIm][OAc], water, and DMSO, as well as the hydrogen bonds between them. Inaccurate modeling of these directed interactions may lead to an imprecise description of the delicate hydrogen bond network. Therefore, we have developed optimized force field parameters for DMSO in this complex mixture to achieve the level of accuracy comparable to quantum chemical MD simulations (*ab initio* MD (AIMD) simulations).

For the investigation of the bio-molecule solution process with force field simulations, we have already published optimized force field parameters for the ionic liquids 1-ethyl-3-methylimidazolium acetate ([EMIm][OAc]) (Roos and Brehm 2021), 1-ethyl-3-methyl-1,2,3-triazolium acetate ([EMTr][OAc]), 1-ethyl-3-methyl-1,2,3-triazolium benzoate ([EMTr][OBz]), 1-ethyl-3-methylimidazolium benzoate ([EMIm][OBz]) (Roos et al. 2023a), water, and cellulose. This article presents the extension of the force field BILFF (Roos and Brehm 2021, Roos et al. 2023b, a) (*B*io-Polymers in *I*onic *L*iquids *F*orce *F*ield) to the co-solvent DMSO. For this purpose, we compared vari-

ous analyses regarding the microstructure and dynamics of the system from force field MD simulations with the results of reference quantum chemical MD simulations and minimized the deviations by varying the force field parameters. This allowed us to develop an optimal parameter set with a focus on the hydrogen bonds of the system simultaneously in anhydrous and aqueous [EMIm][OAc]. For validation, further simulations of pure and aqueous DMSO in the absence of the ionic liquid were calculated and the system densities, self-diffusion coefficients, thermal volume expansion coefficient, and the compressibility were compared with experimental data. In addition, the reproducibility of the quantum chemical results at elevated simulation temperature was investigated. Furthermore, the lifetime of the investigated hydrogen bonds, densities and self-diffusion coefficients were compared with the results from force field simulations of DMSO-free [EMIm][OAc] and thus the influence of DMSO on the system was discussed.

Computational details

The force field parameters for DMSO in mixtures with [EMIm][OAc] were developed simultaneously in both the presence and absence of water at 350 K. The force field parameters were iteratively adjusted by comparing various analyses of the force field MD simulation with reference AIMD simulations (see "Optimization procedure"). The initial configurations for these AIMD simulations were generated from the final configuration of a 20 ns NpT force field simulation with the force field parameters of OPLS–AA (Jorgensen et al. 1996, Ponder and Case 2003, Sambasivarao and Acevedo 2009) for DMSO, BILFF (Roos and Brehm 2021, Roos et al. 2023b, a) for [EMIm][OAc], and TIP4P–EW (Horn et al. 2004) (with constrained bonds and angles using the RATTLE algorithm (Andersen 1983, Ryckaert et al. 1977) for water. The simulation parameters such as the number of molecules, the size of the simulation cell and the final system density are listed in Table 1. The AIMD simulations were performed—analogously to those in our previously published article on the force field parameters for [EMIm][OAc] (Roos and Brehm 2021)—with CP2k (Hutter et al. 2014, Kühne et al. 2020, The CP2K developers group 2017). The Quickstep method (VandeVondele et al. 2005) and orbital transformation (OT) (VandeVondele and Hutter 2003)

were used. For the description of the electronic structure, density functional theory (Hohenberg and Kohn 1964, Kohn and Sham 1965) was applied using the BLYP functional (Becke 1988, Lee et al. 1988) and the dispersion correction D3(BJ) of Grimme et al. (2010, 2011) together with the revised damping parameters of Smith et al. (2016). The DZVP–MOLOPT–SR–GTH (VandeVondele and Hutter 2007) were applied as basis sets, and GTH pseudopotentials (Goedecker et al. 1996, Hartwigsen et al. 1998) were utilized. The plane-wave energy cutoff was set to 350 Ry.
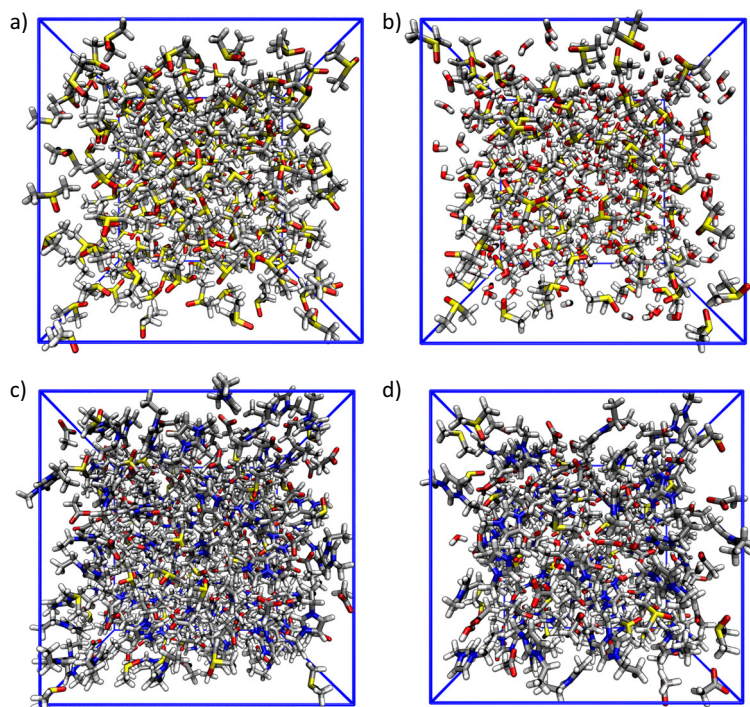
The first 15 ps of the AIMD simulations of the DMSO/IL/(H$_2$O) systems and the first 20 ps of the AIMD simulations of pure DMSO and DMSO/H$_2$O were discarded as equilibration. The resulting physical simulation times are listed in Table 1.

The force field MD simulations for the force field optimization were performed analogously to our previous article on BILFF (Roos and Brehm 2021). Using Packmol (Martínez et al. 2009), the molecules were statistically distributed in the simulation box. Pre-equilibrations were performed at first at 500 K in the NVE ensemble using a Berendsen thermostat (Berendsen et al. 1984) with a coupling constant of 1.0 fs and a physical simulation time of 25 ps, followed by 100 ps of equilibration at 350 K in the NpT ensemble using a Nosé–Hoover thermostat (Martyna et al. 1992, Nose 1984a, b) (coupling constant of 100 fs) and a Nosé–Hoover barostat (coupling constant of 2000 fs). The resulting acoustic shock waves were subsequently damped in another simulation interval with the help of a Langevin thermostat (Dünweg and Paul 1991, Schneider and Stoll 1978). After calculating the final volume of the simulation box as average over the NpT simulation, the simulation cell size was adjusted in a 10 ps simulation interval. In a next step, the shock waves were damped again and the system was equilibrated. Finally, the production run was performed in the NVT ensemble using a Nosé–Hoover thermostat (Martyna et al. 1992, Nose 1984a, b) with a physical simulation time of 10 ns and an integration time step of 0.5 fs. As in our previous studies, the Lennard-Jones cutoff radius was set to 800 pm. For the electrostatic interactions, the PPPM long-range solver from LAMMPS (Plimpton 1995) was utilized.

In addition, to validate the force field, an AIMD simulation and a force field MD simulation of pure and aqueous DMSO at 350 K were performed. To investigate the temperature dependence of the force field,

Table 1 Simulation parameters of the final equilibrated *ab initio* and force field MD simulations of DMSO in pure and aqueous [EMIm][OAc] for development and validation of the force field

System	Number of Molecules	Sim. time / ps	Box size / pm	Density / $g\,cm^{-3}$
AIMD				
DMSO	64 DMSO	90	1962	1.100
DMSO/H_2O	24 DMSO	31	1687	0.947
	48 Water			
DMSO/IL	12 DMSO	135	2052	1.064
	27 IL pairs			
DMSO/IL/H_2O	12 DMSO	120	2055	1.067
	26 IL pairs			
	12 Water			
FFMD				
DMSO	250 DMSO	10 000	3143	1.045
DMSO/H_2O	150 DMSO	10 000	3031	1.022
	300 Water			
DMSO/IL	60 DMSO	10 000	3485	1.086
	135 IL pairs			
DMSO/IL/H_2O	36 DMSO	10 000	2945	1.088
	78 IL pairs			
	36 Water			

Fig. 1 Snapshot of the force field MD simulation of a) pure DMSO, b) aqueous DMSO as well as c) DMSO/IL, and d) DMSO/IL/H_2O (atom color code: yellow – S; red – O; blue – N; gray – C; white – H)

AIMD simulations of DMSO in [EMIm][OAc] and [EMIm][OAc]/water, as well as force field MD simulations of all four systems at an elevated temperature of 450 K, were carried out. After discarding the first 15 ps of the AIMD simulation of the DMSO/IL/(H$_2$O) system for equilibration, the resulting physical simulation lengths of the AIMD simulations at 450 K are 91 ps (DMSO/IL) and 90 ps (DMSO/IL/H$_2$O).

Snapshots of the force field MD simulations of the four different systems are shown in Fig. 1.

The analyses shown in this article were performed with the trajectory analysis program package TRAVIS (Brehm and Kirchner 2011, Brehm et al. 2020b) and visualized using xmgrace (Grace Development Team 1996), Wolfram Mathematica (Wolfram Research, Inc. 2010), and VMD (Humphrey et al. 1996) with the Tachyon renderer (J. Stone 1998). To calculate the lifetime of the hydrogen bonds, the autocorrelation formalism (Rapaport 1983) was applied.

Optimization procedure

In developing the force field parameters for DMSO in [EMIm][OAc], special attention was paid to the hydrogen bonds in the system, in particular the hydrogen bond between the oxygen atom of DMSO and the ring protons of the imidazolium cation. In the literature, the interaction between the cation and DMSO is considered to play an important role for the increased cellulose solubility (Mohan et al. 2016). The DMSO–DMSO interaction was also considered for the force field development. However, since this hydrogen bond is increasingly weakened by the ionic liquid above a molar fraction beyond $\chi_{IL} = 0.46$, its optimization was subordinated to the DMSO–cation hydrogen bond (Paiva et al. 2022).

The force field adjustment was performed simultaneously for both pure and aqueous [EMIm][OAc] at 350 K to also accurately reproduce the interactions of the system for a consideration of the subsequent precipitation process of cellulose with water. A molar fraction of DMSO of $\chi_{DMSO} = 0.31$ was chosen in pure [EMIm][OAc], since at this point the cellulose solubility is sufficiently high (Tomimatsu et al. 2019, Xu et al. 2013).

For DMSO in aqueous [EMIm][OAc], a molar fraction of DMSO of $\chi_{DMSO} = \chi_{water} = 0.24$ (equivalent to 3.9 wt.% water) was determined, since cellulose becomes insoluble in [EMIm][OAc] above 15 wt.% water content even at higher temperature of $323 - 353$ K (Froschauer et al. 2013, Le et al. 2012).

To optimize the force field parameters, the radial and distance–angle distribution functions of the cation–DMSO hydrogen bond calculated from force field MD simulations were compared with reference AIMD simulations.

The force field parameters q and σ for all atoms of DMSO were iteratively adjusted via a trial-and-error method until the deviations of the radial distribution function were minimized.

Furthermore, a comparison of the system density with experimental data was used for the optimization of σ (cf. Table 3). In the ESI†, also a comparison of the partial charges of DMSO with common other literature force fields (Bordat et al. 2003, Fox and Kollman 1998, Geerke et al. 2004, Strader and Feller 2002) based on AMBER (Cornell et al. 1995) and GROMOS (Liu et al. 1995) can be found.

The bonded interactions were adjusted by comparing the statistical occurrence of the bond lengths, angles, and dihedral angles appearing in the reference AIMD simulations with the force field simulations and modifying the corresponding force constants and height of the potential barriers. This resulted in, for example, a modification of the C–S bond length from 179.0 pm to 184.3 pm to reflect the statistically most frequent equilibrium bond length. Furthermore, it should be noted that dihedral angles were not specified in the reference force field OPLS–AA (Jorgensen et al. 1996, Ponder and Case 2003, Sambasivarao and Acevedo 2009) and were introduced in our force field. The nomenclature used for atom types can be found in Fig. 2. All force field parameters are shown in the ESI†.
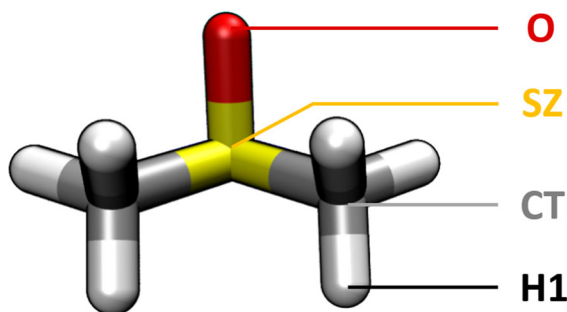
Fig. 2 Nomenclature of atom types in our force field BILFF

Microstructure of the system

Radial distribution functions

To analyze the microstructure, a distribution function of the averaged distances between a reference and an observed particle is calculated. The resulting radial pair distribution function (RDF) gives the probability of finding the observed particle at a given distance from a reference particle, relative to the uniform density of observed particles throughout the simulation cell. In the following, the hydrogen bonding of the different DMSO systems in the presence and absence of water is investigated via RDFs. The reproducibility of the microstructure of the AIMD simulations using BILFF for DMSO is discussed in comparison to the literature force field OPLS–AA (Jorgensen et al. 1996, Ponder and Case 2003, Sambasivarao and Acevedo 2009). Figure 3 shows the RDF between the oxygen atom of DMSO and the ring protons of [EMIm]$^+$ in both the pure and aqueous DMSO/IL systems. The RDFs of the individual hydrogen bonds were averaged over all three ring protons. The oxygen atom of DMSO form a hydrogen bond to the cation [EMIm]$^+$ with a particle distance of about 208 pm and a $g(r) = 1.5 - 1.6$, as can be seen from the first maximum of the RDF. The agreement of the RDF with the AIMD-based result is very good. To achieve this, the partial charge of the DMSO oxygen atom was increased by about 13% from -0.420 to -0.474 compared to the literature force field (Jorgensen et al. 1996, Ponder and Case 2003, Sambasivarao and Acevedo 2009). A comparison between the results of the literature force field and the AIMD simulation shows clear deviations and emphasizes the need for optimization of the force field parameters in order to accurately reproduce the hydrogen bonds. Comparing the DMSO–cation RDF in the presence and absence of water reveals similar residence probabilities, indicating that water does not influence the strength of the hydrogen bonding.

Considering the hydrogen bond between DMSO and water (cf. Fig. 4), a maximum in the RDF calculated from the reference AIMD simulation at a particle distance of about 180 pm and a height of $g(r) = 4.2$ can be observed. While the averaged hydrogen bonding distance between these atoms in the AIMD simulation is correctly reproduced by the force field MD simulation with BILFF and agrees very well with quantum chemical distances calculated in the literature (Kirchner and

Reiher 2002), the residence probability is slightly too low. Nevertheless, the agreement between the results of the reference AIMD simulation and a force field simulation with BILFF is much better than the result calculated with the literature force field. Finding a balance between the accuracy of the description of the complicated interactions between the protons of the cation vs. water and the DMSO oxygen atom is not trivial. However, our main goal is to accurately reproduce the cellulose/[EMIm][OAc]/DMSO system, so we have accepted the deviation in the replication of the DMSO-water hydrogen bond. As a result, the force field parameters of DMSO have not been further modified. A comparison between the DMSO–cation and the DMSO–water hydrogen bond shows a significantly higher $g(r)$ in the second case, which allows conclusions to be drawn about a stronger interaction with water.

In order to verify the transferability of the force field to different concentration ratios of DMSO and water, additional simulations were performed with a mixing ratio of DMSO to water of 1:1. An RDF of the hydrogen bond between DMSO and water can be found in Fig. S–3 in the ESI†. Again, the particle distance from the AIMD simulation can be reproduced correctly, but the height of the $g(r)$ is a little too low.

The analysis of the DMSO–DMSO interactions shows that the $g(r)$ between the DMSO carbon atoms and the protons (see Fig. 5) in the DMSO/IL and DMSO/IL/H$_2$O systems in the AIMD simulation differ slightly from each other. The g(r) of the force field simulation with BILFF lies within the average of these two RDFs. However, the RDF of the hydrogen bond between two DMSO molecules (cf. Fig. S-2) in the force field simulations shows a slight deviation from the AIMD-based results regarding the location and intensity of the initial peak. This difference is observed in both force field simulations utilizing the literature force field and BILFF. It underscores the challenge of accurately capturing the intricate interactions within this complex system.

Combined distance–angle distribution functions

Considering the combined distance–angle distribution functions of two molecules, information is provided whether certain molecule arrangements occur preferentially. Such a combined distribution function (CDF) between an example ring proton of [EMIm]$^+$ and the

Fig. 3 Comparison of the RDFs between the reference AIMD simulation and a force field MD simulation with the OPLS–AA force field (Jorgensen et al. 1996, Ponder and Case 2003, Sambasivarao and Acevedo 2009) and BILFF between the DMSO oxygen atom and the ring protons of [EMIm]$^+$. The RDFs are averaged over all three ring protons
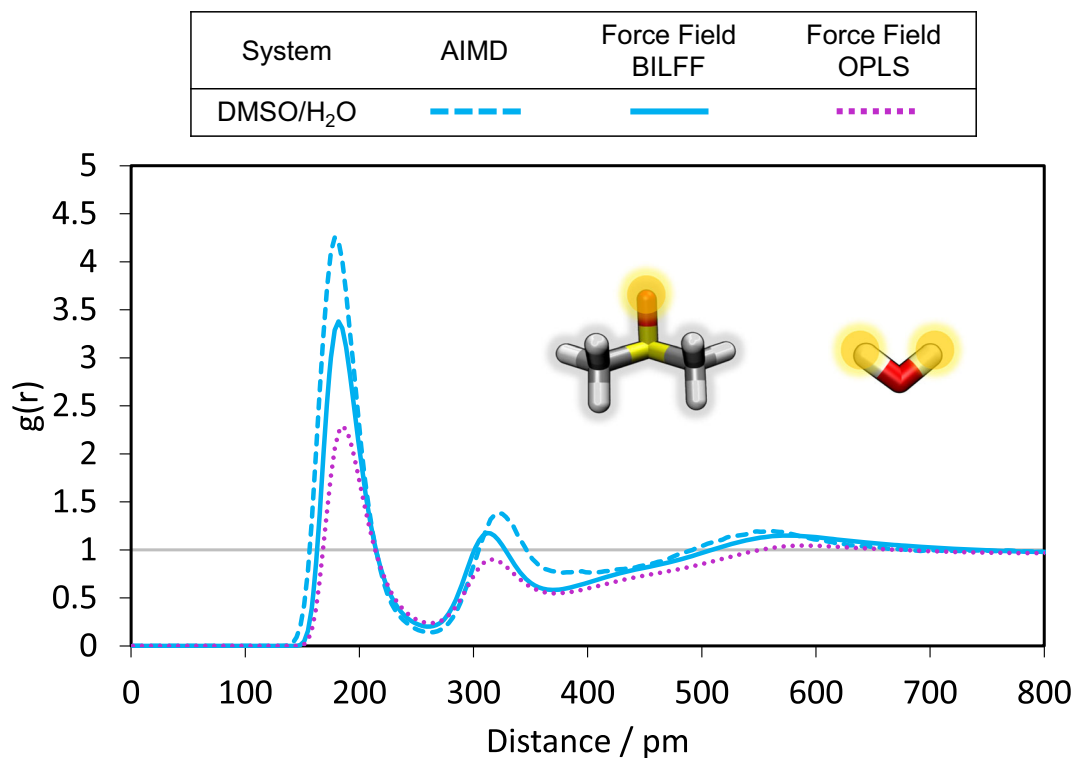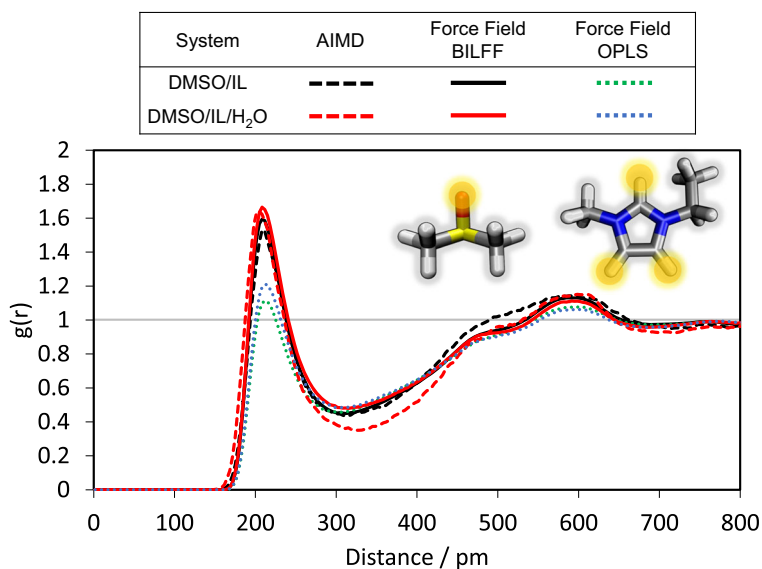
Fig. 4 Comparison of the RDFs between the reference AIMD simulation and a force field MD simulation with the OPLS–AA force field (Jorgensen et al. 1996, Ponder and Case 2003, Sambasivarao and Acevedo 2009) and BILFF between the DMSO oxygen atom and the water protons in the DMSO/H$_2$O system
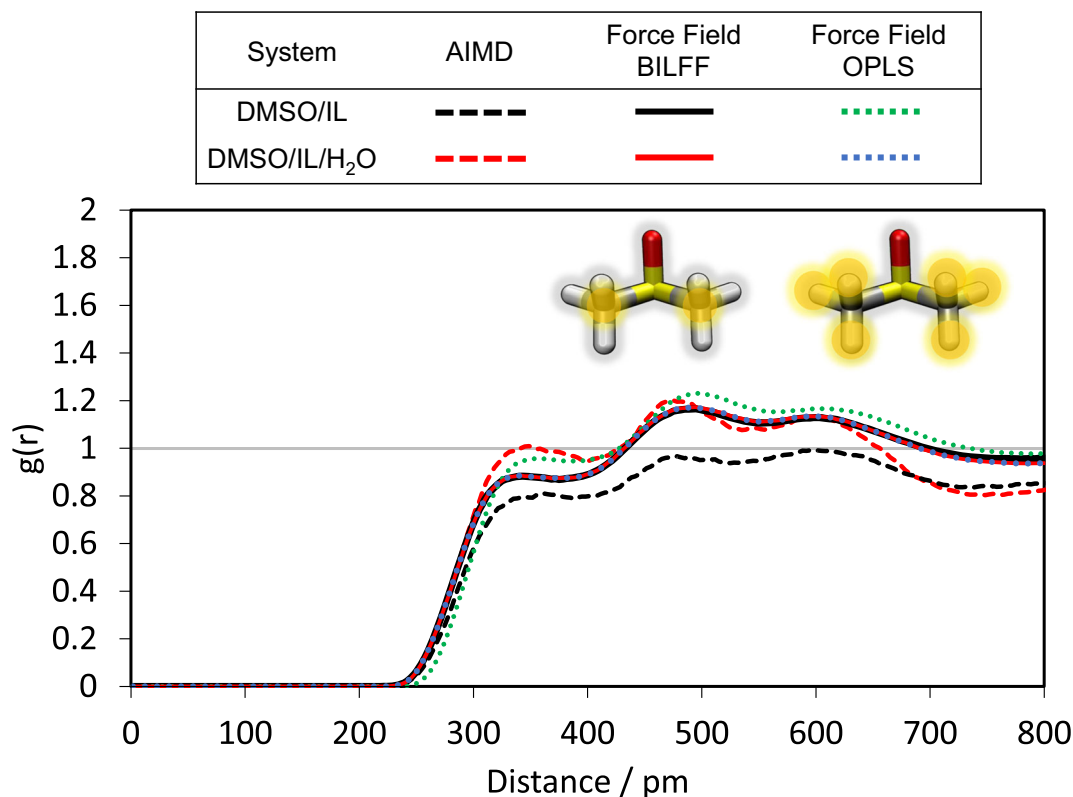
Fig. 5 Comparison of the RDFs between the reference AIMD simulation and a force field MD simulation with the OPLS–AA force field (Jorgensen et al. 1996, Ponder and Case 2003, Sambasivarao and Acevedo 2009) and BILFF between the DMSO carbon atom and the DMSO protons

DMSO oxygen atom is presented in Fig. 6 showing the distance $O_{DMSO} \cdots H_{EMIm}$ and the corresponding angle $\angle(O_{DMSO}, CH_{EMIm}, H_{EMIm})$ as depicted in the illustration. The CDF of the AIMD simulation (top) and the FFMD simulation with BILFF (bottom) exhibit a strong overall agreement. The peak at $80-280$ pm, $117-180°$ represents the hydrogen bond between the two molecules. Here, the force field MD simulation depicts a slightly wider angle range, plausibly due to a better statistical sampling than the AIMD simulation. The second peak ($395-520$ pm, $50-80°$) corresponds to the hydrogen bonding involving the isolated CH group of $[EMIm]^+$, resulting in an increased presence of DMSO on the "opposite" side of $[EMIm]^+$.

Considering the CDF of DMSO and water (cf. Fig. 7), a similar good agreement of the overall pattern can be obtained between the results of the AIMD and FFMD simulations. The first peak ($30-240$ pm, $145-180°$) shows the hydrogen bond between DMSO and water. The second maximum at $295-350$ pm and $40-70°$ arises from the "second" water proton. Again, the AIMD simulation infers a marginally stronger localization than the force field.

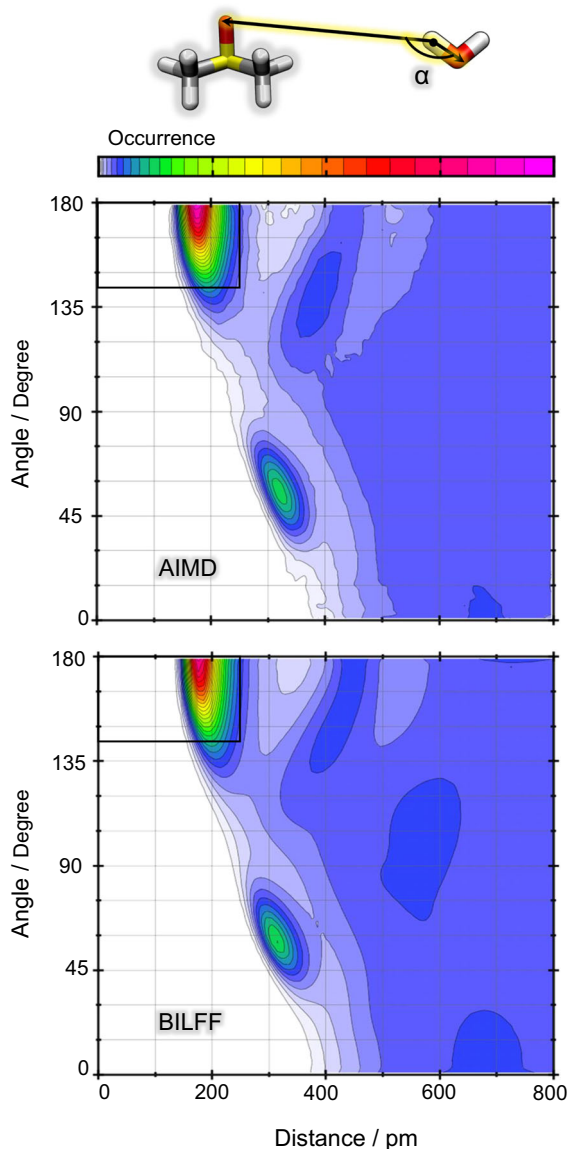*Spatial distribution functions*

The microstructure of the system can be further investigated using spatial distribution functions (SDFs). Figure 8 shows the arrangement of the different compounds in the DMSO/IL/H$_2$O system around a DMSO molecule, where preferential orientations can be identified. Around the oxygen atom of a DMSO molecule, protons from neighboring DMSO molecules (shown in gray), $[EMIm]^+$ cations (shown in red), and water (shown in blue) are arranged in a circular formation in layers, resulting from the directional dependence of hydrogen bonding and the free rotation of the DMSO oxygen atom. Here, the competition of the
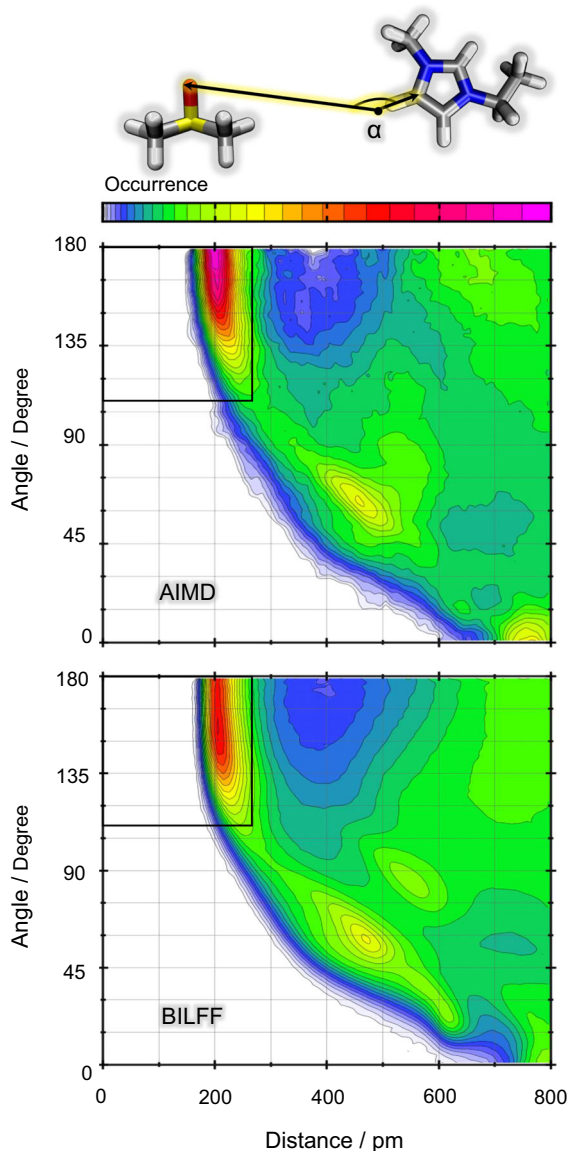
Fig. 6 Distance–angle distribution function between an example ring proton of [EMIm]$^+$ and the DMSO oxygen atom in the DMSO/IL system comparative as a result of a reference AIMD simulation and a force field MD simulation with BILFF. The black rectangle shows the geometric criterion for calculating the lifetime of the hydrogen bonds. The depicted angle is for illustrative purposes only

Fig. 7 Distance–angle distribution function between the protons of water and the DMSO oxygen atom in the DMSO/H$_2$O system comparative as a result of a reference AIMD simulation and a force field MD simulation with BILFF. The black rectangle shows the geometric criterion for calculating the lifetime of the hydrogen bonds. The depicted angle is for illustrative purposes only

hydrogen bond donors for the acceptor oxygen atom of DMSO becomes apparent, which is also discussed in the Sankey diagrams in Figs. 10 and 11. Within the molecule layers around the DMSO oxygen atom, a water bi-layer is formed around [EMIm]$^+$, resulting in being isolated from DMSO.
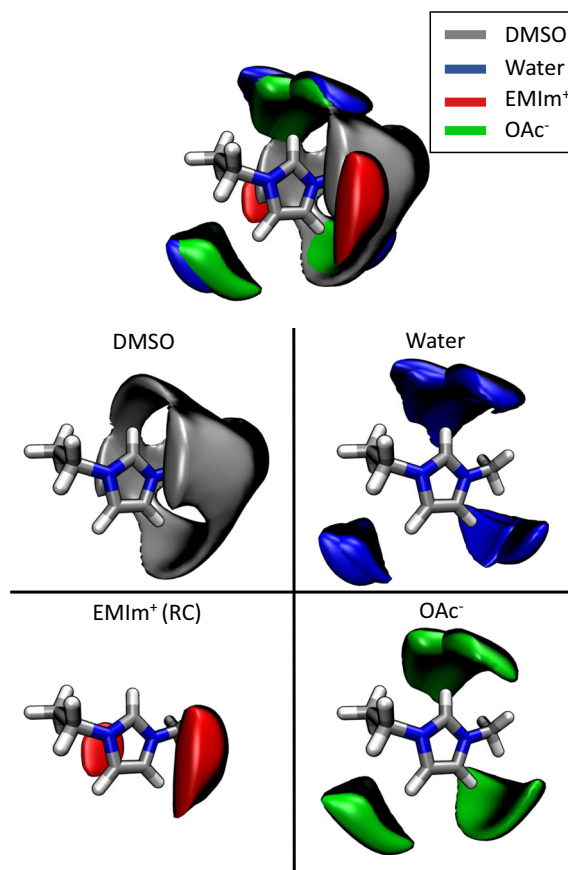
The protons of a DMSO molecule are surrounded by acetate (shown in green), water (shown in blue), and other DMSO molecules (shown in gray) in a competitive manner. The directed interactions of the hydrogen bonding partners, combined with the repulsion associated with the dihedral angles and the rotational free-
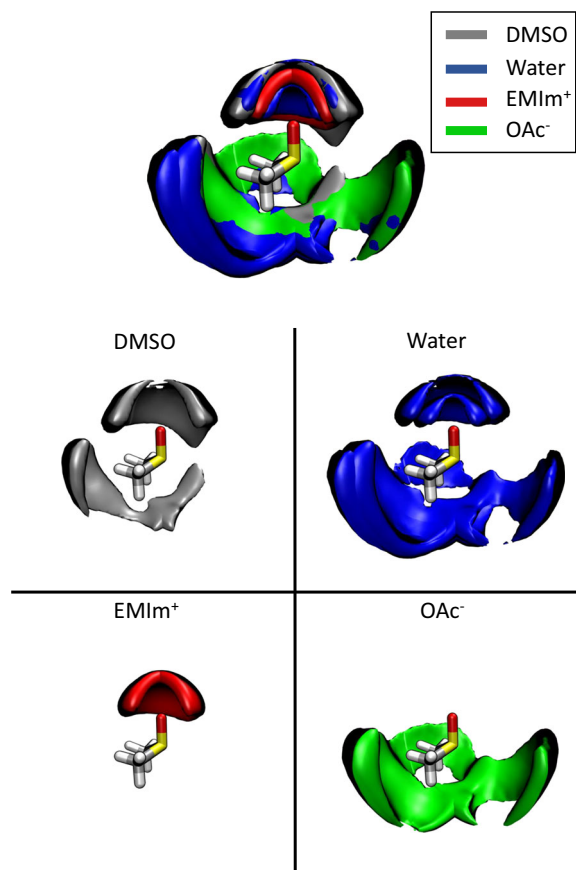
Fig. 8 Spatial distribution function (SDF) of the arrangement of molecules around DMSO with protons and oxygen atoms of DMSO (gray, oxygen: $4\,\mathrm{nm}^{-3}$; proton: $2\,\mathrm{nm}^{-3}$) and water (blue, $2.5\,\mathrm{nm}^{-3}$), the ring protons of [EMIm]$^+$ (red, $5\,\mathrm{nm}^{-3}$) and the oxygen atom of acetate (green, $5\,\mathrm{nm}^{-3}$) in the DMSO/IL/H$_2$O system calculated with BILFF

Fig. 9 Spatial distribution function (SDF) of the arrangement of molecules around [EMIm]$^+$ with the protons and oxygen atoms of DMSO (gray, $3\,\mathrm{nm}^{-3}$) and water (blue, $6\,\mathrm{nm}^{-3}$), the ring center of [EMIm]+ (red, $7\,\mathrm{nm}^{-3}$) and the oxygen atom of acetate (green, $10\,\mathrm{nm}^{-3}$) in the DMSO/IL/H$_2$O system calculated with BILFF

dom of the methyl groups in DMSO, result in a circular alignment of these molecules in three distinct regions.

A consideration of the spatial distribution functions of the neighboring molecules around an [EMIm]$^+$ cation (cf. Fig. 9) shows that DMSO arranges nearly uniformly around the cation without a preferred orientation. This is in contrast to the orientation of the oxygen atoms of water and acetate around the ring protons of [EMIm]$^+$ as well as an orientation of the ring center of the next cation in top of one another due to $\pi-\pi$-stacking. These results are in agreement with the observations for the [EMIm][OAc]–water system in the absence of DMSO, which were discussed in our previously published article on BILFF (Roos and Brehm 2021). Thus, the presence of DMSO in the aqueous

ionic liquid does not significantly change the arrangement of the anion and water around the cation, though it does compete with the hydrogen bonds of the anion and water for the cation, which will be discussed in the following section.

The SDFs calculated from the reference AIMD simulations can be found in the ESI†(cf. Figs. S-4 and S-5).

Competing hydrogen bonds

The multiple hydrogen bond donors and acceptors in the quaternary system of DMSO, [EMIm][OAc] and water engage in a competition with one another. In order to analyze the intricate network of the hydrogen bonds, Sankey diagrams are used (cf. Figs. 10 and 11).

Fig. 10 Sankey diagram of DMSO in anhydrous [EMIm][OAc] calculated from a force field MD simulation using BILFF with a comparison to the coordination numbers from a reference AIMD simulation
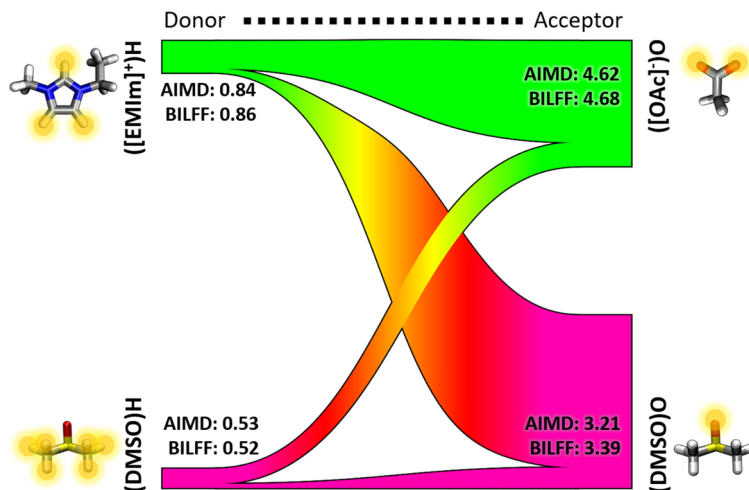
Fig. 11 Sankey diagram of DMSO in aqueous [EMIm][OAc] calculated from a force field MD simulation using BILFF with a comparison to the coordination numbers from a reference AIMD simulation
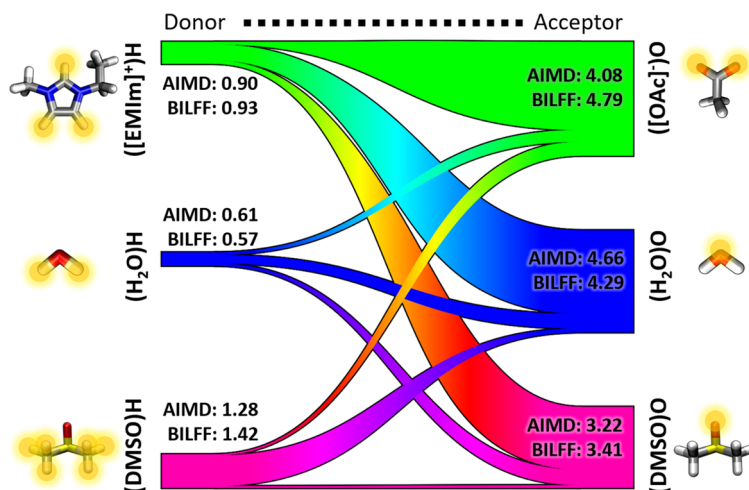
Fig. 12 Radial distribution function of the hydrogen atoms of $[EMIm]^+$ averaged over all ring protons, with the oxygen atom of DMSO in the anhydrous DMSO/IL system at 350 and 450 K simulated by AIMD and FFMD using BILFF
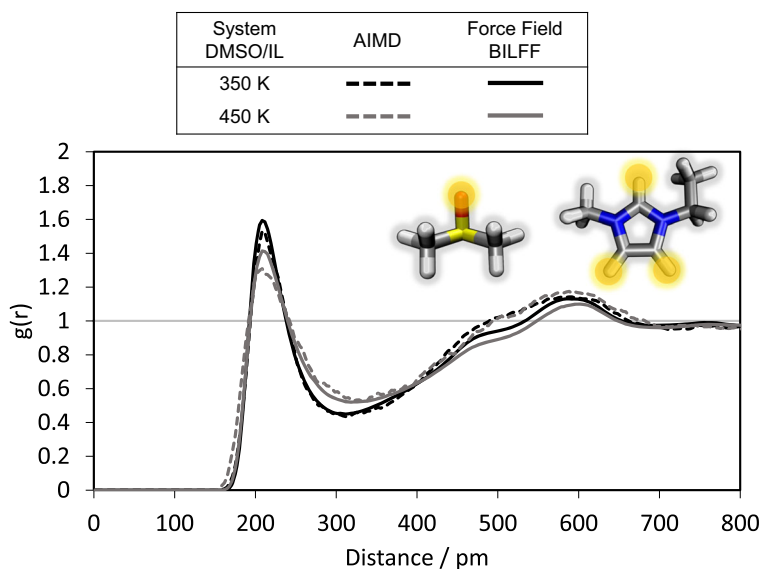
The left side of the diagram shows the hydrogen bond donors, while the right side corresponds to the hydrogen bond acceptors. The width of the bars is proportional to the number of hydrogen bonds that are formed per donor/acceptor site on average. The numbers in the bars represent the coordination numbers and result from the number integral of the corresponding RDFs up to the first minimum. In the anhydrous DMSO/IL system (cf. Fig. 10), it is obvious that hydrogen bonds are formed mainly between $[EMIm]^+$ and $[OAc]^-$ but DMSO competes strongly as a hydrogen bond acceptor. Thus, the oxygen atom of $[OAc]^-$ is surrounded by about 5 protons of mostly $[EMIm]^+$, but also of other DMSO molecules. The DMSO oxygen atom, on the other hand, is surrounded by 3 protons of other molecules. This finding is in agreement with literature simulations (Paiva et al. 2022). Similar results are found in the presence of water (cf. Fig. 11). The coordination number of the DMSO protons calculated from the force field MD simulation increases from 0.52 in the anhydrous system to 1.42 in the aqueous system. This is due to the hydrate shell around DMSO. The competition for the protons of $[EMIm]^+$, formerly between $[OAc]^-$ and DMSO, is now dominated by water.

The coordination numbers from the AIMD simulations, and thus the microstructure of the systems, can be well reproduced by force field simulations using BILFF in both the presence and absence of water.

Temperature dependence

Radial distribution functions at higher temperatures

BILFF was developed at a temperature of 350 K for DMSO in anhydrous and aqueous [EMIm][OAc]. For validation at different temperatures, force field MD simulations with the same simulation parameters (cf. Table 1) were performed at 450 K. In addition, force field MD simulations of anhydrous and aqueous DMSO were performed and included in the validation of our force field.

The radial distribution functions of the ring protons of $[EMIm]^+$ and the oxygen atom of DMSO in the anhydrous and aqueous DMSO/IL system are compared with RDFs calculated from the AIMD simulation (cf. Figs. 12 and 13). As expected, the residence probability $g(r)$ of the observed atoms is decreasing with increasing temperature in both systems. The average distance between the molecules, which is in both systems at around 210 pm, is not affected by temperature.

The force field simulation with our optimized parameters can also reproduce the results of the AIMD simulation at 450 K.

Hydrogen bond lifetime

In order to describe the microstructure of the systems and to validate BILFF, several structural quan-

Fig. 13 Radial distribution function of the hydrogen atoms of $[EMIm]^+$, averaged over all ring protons, with the oxygen atom of DMSO in the aqueous DMSO/IL system at 350 and 450 K simulated by AIMD and FFMD using BILFF
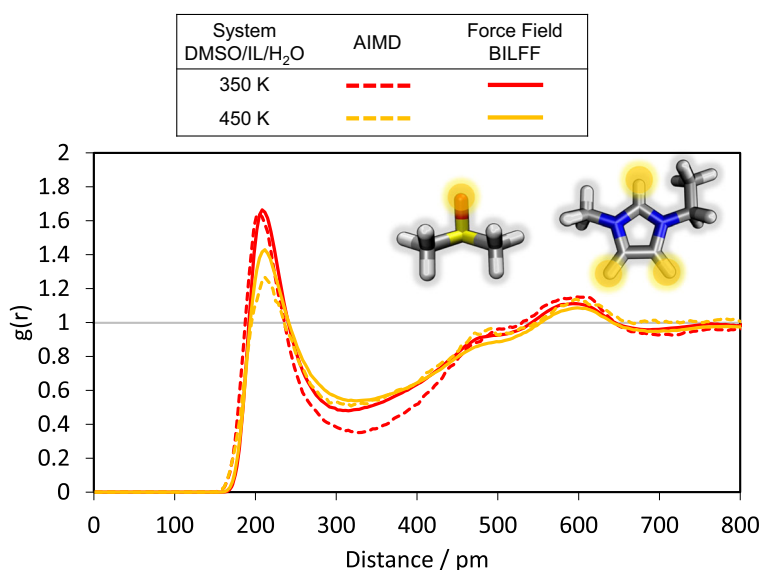
tities have been investigated so far. To further analyze the dynamics, we performed hydrogen bond lifetime calculations at two different temperatures and compared the results for six different systems, including anhydrous DMSO, aqueous DMSO, DMSO–[EMIm][OAc], DMSO–[EMIm][OAc]–water, and anhydrous and aqueous [EMIm][OAc]. Additionally, we compared the results of force field MD simulations with BILFF to the AIMD simulation.

Table 2 shows the lifetime of the most relevant hydrogen bonds of the molecules in the investigated systems at 350 K and 450 K resulting from AIMD simulations as well as force field simulations using BILFF. A distinction was made between the calculation of a continuous and intermittent hydrogen bond lifetime. While the intermittent lifetime allows breaking and reformation of hydrogen bonds, the continuous lifetime only considers hydrogen bonds without interruption in the autocorrelation. The distance and angle criteria between the hydrogen bond partners of interest were selected according to the maximum probability of residence in the combined distance–angle distribution function and are tabulated in the ESI†(cf. Table S-7). An example of the determination of these criteria is given in Figs. 6 and 7 as shown by the black rectangle in the CDFs.

The results of the lifetime calculation for the hydrogen bonds of the individual ring protons of [EMIm]$^+$ are also listed in the ESI†(cf. Table S-8). The following general conclusions can be drawn from the lifetime of the hydrogen bonds:

- As expected, a significant decrease in hydrogen bond lifetime can be observed with increasing temperature and thus a decrease in their stability.
- In any case, the hydrogen bond lifetime until the first interruption (the continuous lifetime) lasts only a few picoseconds, which is a typical time interval for hydrogen bonds (Brehm and Sebastiani 2018, Gehrke et al. 2018, Roos and Brehm 2021).
- The water–anion and the cation–anion hydrogen bonds generally have the longest observed lifetimes and thus the largest stability in all four systems studied.
- In the presence of DMSO, the intermittent lifetimes of the cation–anion, water–anion, and cation–water hydrogen bonds in the aqueous systems are significantly increased by a factor of up to more than two compared to the systems without DMSO in our previously published article (Roos and Brehm 2021). However, in the anhydrous system, the presence of DMSO reduces the lifetime of the cation–anion hydrogen bond.

Table 2 Overview of the lifetime τ of hydrogen bonds in the AIMD simulation and the force field MD simulation using BILFF at different temperatures. Lifetimes in ps

Temp.	Intermittent		Continuous	
	τ(AIMD)	τ(FFMD)	τ(AIMD)	τ(FFMD)
DMSO				
(DMSO)H-O(DMSO)				
350 K	22.79	22.33	1.82	1.38
450 K	–	7.04	–	0.95
DMSO / H$_2$O				
(DMSO)H-O(DMSO)				
350 K	12.17	23.01	1.27	1.07
450 K	–	5.24	–	0.76
(H$_2$O)H−O(DMSO)				
350 K	45.54	32.92	3.86	5.48
450 K	–	6.93	–	1.81
DMSO / [EMIm][OAc]				
(DMSO)H-O(DMSO)				
350 K	52.55	121.08	2.10	1.54
450 K	26.74	20.20	1.18	1.00

Table 2 continued

Temp.	Intermittent		Continuous	
	τ(AIMD)	τ(FFMD)	τ(AIMD)	τ(FFMD)
([EMIm])H−O(DMSO)				
350 K	64.06	95.21	2.02	2.40
450 K	(103.69)	17.88	0.92	1.28
([EMIm])H−O([OAc])				
350 K	424.66	547.30	4.12	4.78
450 K	48.88	86.59	1.69	2.11
DMSO / [EMIm][OAc] / H_2O				
(DMSO)H-O(DMSO)				
350 K	114.34	118.41	2.22	1.52
450 K	19.07	18.05	0.81	0.98
([EMIm])H−O(DMSO)				
350 K	78.17	93.75	2.13	2.31
450 K	19.95	15.99	0.91	1.24
([EMIm])H−O([OAc])				
350 K	164.51	436.43	2.92	3.97
450 K	57.04	67.32	1.40	1.89
([EMIm])H−O(H_2O)				
350 K	34.89	99.74	0.73	0.93
450 K	14.63	13.99	0.43	0.59
(H_2O)H−O(DMSO)				
350 K	(12.98)	141.73	0.38	3.71
450 K	79.99	19.31	0.71	1.48
(H_2O)H−O([OAc])				
350 K	443.35	455.55	0.02	0.20
450 K	34.49	27.22	0.02	0.15
[EMIm][OAc] [a]				
([EMIm])H−O([OAc])				
350 K	471.98	779.74	2.95	4.45
450 K	87.72	95.83	1.61	1.95
[EMIm][OAc] / H_2O [a]				
([EMIm])H−O([OAc])				
350 K	73.15	146.00	1.26	1.83
450 K	37.75	23.96	2.33	1.12
([EMIm])H−O(H_2O)				
350 K	31.18	40.36	0.57	0.75
450 K	9.81	5.70	0.40	0.50
(H_2O)H−O([OAc])				
350 K	153.15	165.65	0.16	0.78
450 K	44.89	19.83	0.10	0.45

[a] *Calculated from the MD simulations of our already published article* (Roos and Brehm 2021) *with the same angle and distance criteria*

– A consideration of the hydrogen bonds of the individual ring protons of [EMIm]$^+$ shows that the ring proton H2 (between both nitrogen atoms) forms longer lasting hydrogen bonds to water and [OAc]$^-$ than the other two ring protons H4 and H5 (cf. Table S-8 in the ESI†). This is in agreement with the results of a DMSO-free IL/(H$_2$O) system (Roos and Brehm 2021). However, the [EMIm][OAc]–DMSO hydrogen bonds are not affected by this phenomenon.

– The DMSO–H$_2$O hydrogen bonds are longer-lived than the DMSO–DMSO hydrogen bonds.

– The presence of water decreases the lifetime and thus the stability of the cation–anion hydrogen bond. This is also the case in the DMSO-free system (Roos and Brehm 2021). However, the DMSO hydrogen bonds are not significantly affected.

The AIMD-based results can be reproduced well in the case of the continuous hydrogen bond lifetime. Larger deviations occur for the intermittent hydrogen bond lifetime. On the one hand, dynamical properties—and in particular hydrogen bond lifetimes—are very sensitive to both the experimental conditions and the potential energy surface, which is defined by the force field parameters. Due to this high sensitivity, values can easily be off by an order of magnitude, and the agreement found here is still within acceptable limits (Gehrke et al. 2018, Kohagen et al. 2011, Malberg et al. 2013). On the other hand, it is noteworthy that certain lifetimes exceed the total simulation time of the AIMD simulations ($\approx$ 100 ps). While this is in principle possible via Rapaport's autocorrelation formalism, these AIMD-based values bear a large uncertainty and should be considered rough estimates. The force field simulations, on the other hand, are certainly long enough so that we can report the force field-based hydrogen bond lifetimes with greater confidence.

Validation with respect to experiment

To further validate our optimized force field, the densities, self-diffusion coefficients, thermal volume expansion coefficient, and bulk modulus were investigated and compared to experimental data. In addition, the effect of DMSO on the self-diffusion coefficients is investigated by comparison with DMSO-free [EMIm][OAc] systems (Roos and Brehm 2021).

A consideration of the densities of the different systems shows that the density of DMSO is significantly influenced by the addition of water and the ionic liquid (cf. Table 3). Comparing the density with literature results (Ciocirlan and Iulian 2012, Paknejad et al. 2019) shows an excellent reproduction of the density of pure DMSO at 350 K (cf. Table 3). The deviation is less than 1%. At 450 K, the calculated system density from the force field simulation is slightly lower than experimental data (Paknejad et al. 2019), but is still within an acceptable range with a deviation of 4.7%.

In aqueous DMSO, the calculated system density can also reproduce the experimental data with a deviation of less than 3.8%, given that it was measured at a lower temperature of 338 K with a slightly different molar ratio than used in ref. Cowie and Toporowski (1961) and ref. Lü et al. (2016). Although the force field was not optimized for pure and aqueous DMSO, the nevertheless good agreement of the system density with experimental data further validates the force field.

The density of the DMSO/IL system is in excellent agreement with experimental data (Nisa et al. 2019) and is replicated without any deviation.

As shown in our previous publication (Roos and Brehm 2021), the density of [EMIm][OAc] in water can be well reproduced using BILFF. To our knowledge, no literature values of the density for the complex DMSO/IL/H$_2$O system were published in a comparable temperature and concentration range. But given that the density of DMSO, DMSO/H$_2$O as well as DMSO/IL and IL/H$_2$O show a good agreement with experimental data, it can be assumed that the calculated density of the aqueous DMSO/IL system is also in a realistic range.

In all four systems, simulations utilizing the literature force field OPLS–AA (Jorgensen et al. 1996, Ponder and Case 2003, Sambasivarao and Acevedo 2009) exhibit a slightly too low system density when compared to experimental data.

Furthermore, self-diffusion coefficients at a temperature of 350 K and 450 K were calculated based on the mean squared displacement (MSD) using the Einstein equation and are shown in Table 4. The resulting diffusion coefficients allow the following conclusions:

– In all systems, the self-diffusion coefficient increases with increasing temperature as expected.

– In general, the diffusion coefficients in DMSO/IL/(H$_2$O) are increased compared to DMSO-free IL/(H$_2$O), which were considered in our previously published article (Roos and Brehm 2021).

Table 3 Comparison of the system densities from force field MD simulations (FFMD) using the literature force field OPLS–AA (Jorgensen et al. 1996, Ponder and Case 2003, Sambasivarao and Acevedo 2009) and BILFF with experimental data at two different temperatures

Temperature	Box size / pm	ρ(OPLS) /g·cm^{-3}	ρ(BILFF) / g·cm^{-3}	ρ(Lit.) / g·cm^{-3}
DMSO				
350 K	3142.57	0.99	1.05	1.04 [a] / 1.04 [b]
450 K	3305.94	–	0.90	0.94 [c]
DMSO / H$_2$O				
350 K	3030.53	0.98	1.02	1.06 [d] / 1.06 [e]
450 K	3193.82	–	0.87	–
DMSO / [EMIm][OAc]				
350 K	3496.76	1.06	1.07	1.07 [f]
450 K	3599.64	–	0.99	–
DMSO / [EMIm][OAc] / H$_2$O				
350 K	2953,89	1.07	1.08	–
450 K	3041.72	–	0.99	–

The molar fractions are χ_{DMSO}=0.33 in the DMSO/H$_2$O system and χ_{DMSO}=0.31 in the DMSO/IL mixture

[a] *Measurements at 353.15 K from ref. Ciocirlan and Iulian (2012).*

[b] *Measurements at T=353.15 K from ref. Paknejad et al. (2019).*

[c] *Measurements at T=453.15 K from ref. Paknejad et al. (2019).*

[d] *Measurements at T=338.15 K with a molar fraction of DMSO of x_{DMSO}=0.349 from ref. Cowie and Toporowski (1961).*

[e] *Measurements at T=338.15 K with a molar fraction of DMSO of x_{DMSO}=0.349 from ref. Lü et al. (2016).*

[f] *Measurements at T=353.15 K with a molar fraction of DMSO of x_{DMSO}=0.294 from ref. Nisa et al. (2019)*

Table 4 Self-diffusion coefficients D from force field MD simulations using BILFF of pure and aqueous DMSO as well as DMSO in pure and aqueous [EMIm][OAc] at different temperatures

	Temperature	D(FFMD) / 10^{-11} m^2 s^{-1}	D(Lit.) / 10^{-11} m^2 s^{-1}
DMSO			
DMSO	350 K	171.8	126.4 [a]
DMSO / H$_2$O			
DMSO	350 K	114.5	65.0 [b]
	450 K	581.7	–
H$_2$O	350 K	200.9	110.0 [b]
	450 K	1038.7	–
DMSO / [EMIm][OAc]			
DMSO	350 K	27.5	31.4 [c]
	450 K	158.3	–
[EMIm]$^+$	350 K	16.2	20.6 [c]
	450 K	112.0	–
[OAc]$^-$	350 K	14.0	20.2 [c]
	450 K	86.7	–

Table 4 continued

	Temperature	D(FFMD) / $10^{-11}\,\mathrm{m^2\,s^{-1}}$	D(Lit.) / $10^{-11}\,\mathrm{m^2\,s^{-1}}$
DMSO / [EMIm][OAc] / H$_2$O			
DMSO	350 K	26.3	–
	450 K	196.0	–
[EMIm]$^+$	350 K	17.4	–
	450 K	102.7	–
[OAc]$^-$	350 K	11.7	–
	450 K	95.8	–
H$_2$O	350 K	19.7	–
	450 K	183.6	–
[EMIm][OAc] [f]			
[EMIm]$^+$	350 K	9.26	14[d] / 0.98[e]
	450 K	81.76	311[d]
[OAc]$^-$	350 K	6.72	13[d] /0.84[e]
	450 K	66.83	307[d]
[EMIm][OAc] / H$_2$O [f]			
[EMIm]$^+$	350 K	21.77	4.17[e]
	450 K	171.09	–
[OAc]$^-$	350 K	22.42	4.61[e]
	450 K	155.76	–
H$_2$O	350 K	55.97	10.47[e]
	450 K	378.47	–

The molar fractions in the simulations are χ_{DMSO}=0.33 in DMSO–H$_2$O, χ_{DMSO}=0.31 in DMSO/IL and χ_{DMSO}=0.24 in DMSO/IL/H$_2$O. For comparison, the diffusion coefficients of DMSO-free [EMIm][OAc] and [EMIm][OAc]/H$_2$O are also shown from our previously published article (Roos and Brehm 2021)

[a] *Measurements at 328.15 K from ref.* Holz et al. (2000)

[b] *Measurements at T=308.2 K and* χ_{DMSO}*=0.3 from ref.* Packer and Tomlinson (1971)

[c] *Extrapolated to 350 K via Arrhenius plot from temperature-dependent experimental measurements at T=283–333 K, see ref.* Radhi et al. (2015)

[d] *Linearly extrapolated values of temperature dependent measurements at 283 – 333 K from ref.* Green et al. (2017)

[e] *Measurement at T=313.15 K with a molar fraction of [EMIm][OAc] of* χ_{IL}*=0.3 in the aqueous system* (Hall et al. 2012)

[f] *Calculated values of force field simulations with BILFF at 350 K from our previously published article* (Roos and Brehm 2021). χ_{IL}*=0.25 in the aqueous system*

- In the pure and aqueous DMSO/IL mixture, the self-diffusion coefficients are lower than in both DMSO systems without ionic liquid. Accordingly, the ionic liquid reduces the diffusion rate of DMSO.
- Considering the simulations at a temperature of 350 K, water also lowers the diffusion coefficient of DMSO. This is consistent with the increase of density in the presence of the ionic liquid and water (cf. Table 3) although the viscosity decreases (Le et al. 2014).
- The decrease in the diffusion rate caused by water in a DMSO/IL/H$_2$O mixture at 350 K thereby shows

the opposite effect to the increase of diffusion in DMSO-free IL/H$_2$O (Roos and Brehm 2021), demonstrating the complexity of the underlying hydrogen bond network.

- In both anhydrous and aqueous DMSO/IL, the calculated self-diffusion coefficient of DMSO is slightly larger than the self-diffusion coefficients of [EMIm]$^+$ and [OAc]$^-$, which is in agreement with experimental values for anhydrous DMSO/IL (Radhi et al. 2015). The cation diffuses faster than the anion at both temperatures. Furthermore, water molecules diffuse faster than [EMIm][OAc] but

Fig. 14 Calculation of the thermal volume expansion coefficient γ of the DMSO/IL system at 350 K from multiple FFMD simulations using BILFF at constant pressure (1 bar) and different temperatures
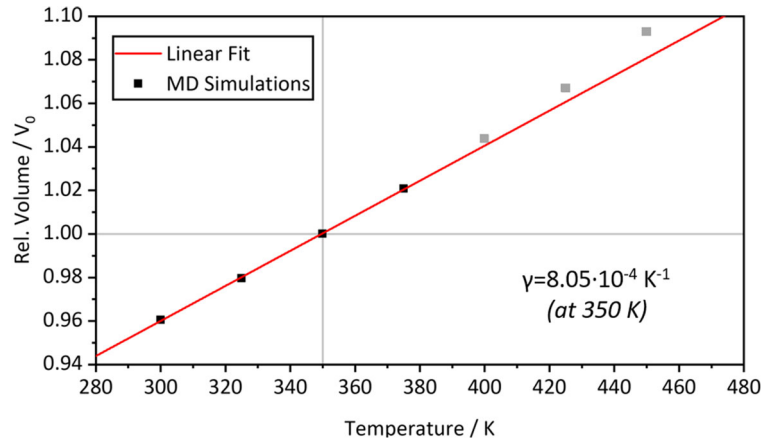
slower than DMSO in the DMSO/IL/H$_2$O mixture, while in the absence of the ionic liquid, water shows a significantly higher diffusion coefficient.

The results of the force field MD simulations with BILFF reflect the general patterns observed in the experimental data. Despite occasional numerical fluctuations in the individual diffusion values and slightly different temperatures and molar fractions of DMSO in the measurements, the overall agreement of this dynamic parameter with the experimental results remains acceptable. The temperature dependence is replicated across a range spanning more than one order of magnitude. It should be noted that especially the quaternary mixture DMSO/[EMIm][OAc]/water has been little studied so far, so no experimental data are available.

All validations discussed above were focused on the microscopic structure and dynamics of the liquid, which is the main aim of our force field. However, to

obtain a more complete picture, we also performed a few validations based on (macroscopic) thermodynamic properties, as it will be discussed in the following.

The bulk modulus of pure DMSO (cf. Fig. 14) and the thermal expansion coefficient of the DMSO/IL system (cf. Fig. 15) were calculated and compared with experimental data. For this purpose, force field simulations were performed in the NpT ensemble at different temperatures/pressures, and the relative volume change was represented as a graph. The two quantities were calculated using a linear fit to the results close to a temperature of 350 K and a pressure of 1 bar and were compared to experimental data in Table 5. The compressibility was measured at 353.15 K and 5 bar (Paknejad et al. 2019) as well as at a temperature of 323.15 K and a pressure of 1.01 bar (Egorov et al. 2010). The thermal expansion coefficient for the DMSO/IL mixture was measured at 353.15 K and a molar fraction

Fig. 15 Calculation of the compressibility κ and the bulk modulus K of pure DMSO at 1 bar from multiple FFMD simulations using BILFF at constant temperature (350 K) and different pressures
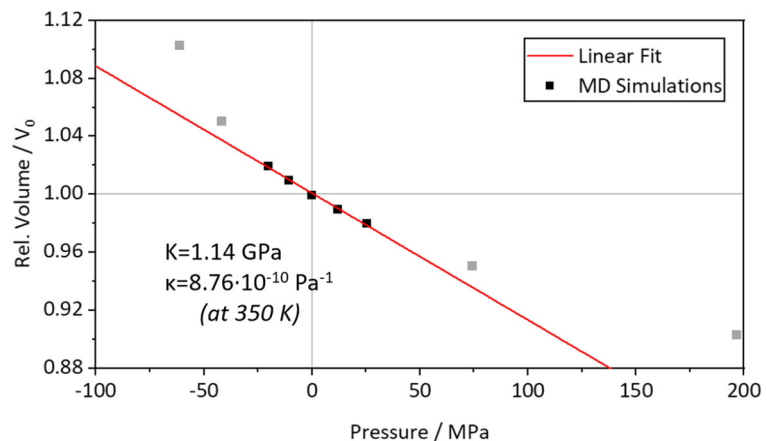
Table 5 Comparison of the calculated compressibility κ of a force field MD simulation using BILFF of pure DMSO and the calculated thermal expansion coefficient γ of DMSO in [EMIm][OAc] (χ_{IL}=0.69) at 350 K and 1 bar with experimental data (Egorov et al. 2010, Paknejad et al. 2019, Yang et al. 2019a)

	FFMD	Experiment
DMSO		
Compressibility κ / $10^{-10}\,Pa^{-1}$	8.76	7.35 [a] / 7.04 [b]
DMSO/[EMIm][OAc]		
Thermal expansion coeff. γ / $10^{-4}\,K^{-1}$	8.05	6.10 [c]

[a] *Measurements at 353.15 K and 5 bar from ref.* Paknejad et al. (2019).

[b] *Measurements at T=323.15 K and 1.01 bar from ref.* Egorov et al. (2010).

[c] *Measurements at T=353.15 K and χ_{IL}=0.65 from ref.* Yang et al. (2019a).

Table 6 Experimental and computed enthalpy of vaporization ΔH_{Vap} of pure DMSO at 293 K and 1 bar, including the pV work term $p\Delta V \approx 2.3\,kJ\,mol^{-1}$. Experimental data taken from ref. Douglas (1948)

	ΔH_{Vap} / $kJ\,mol^{-1}$
Experiment [a]	52.89 ± 0.42
Simulation (BILFF)	54.14
Simulation (OPLS–AA)	51.13

[a] *Measurement at 298.15 K from ref.* Douglas (1948)

of the ionic liquid of χ_{IL}=0.647 according to ref. Yang et al. (2019a).

A comparison of the calculated values for the compressibility of pure DMSO and the thermal expansion coefficient of DMSO in [EMIm][OAc] with experimental data shows a good agreement, although the thermal expansion was measured at a 30 K lower temperature and the force field was not optimized for pure DMSO. In addition to the density (cf. Table 3) and the self-diffusion coefficient (cf. Table 4), also these two quantities can be well reproduced by BILFF for both pure DMSO as well as a DMSO/IL mixture.

The final validation which we performed concerns the enthalpy of vaporization ΔH_{Vap} of pure DMSO. We have used the following computational protocol. During a liquid phase simulation of pure DMSO in *NpT* ensemble, we averaged the total potential energy of the system, which is equivalent to the internal energy U_{liquid}. In addition, we performed a set of simulations of one DMSO molecule in vacuum, starting from different initial configurations, and also averaged the potential energy, which corresponds to U_{gas}. Based on these results, we were able to obtain the internal energy of vaporization $\Delta U_{Vap} = U_{gas} - U_{liquid}$. The final step to the enthalpy is given via $\Delta H_{Vap} = \Delta U_{Vap} + p\Delta V$. From the experimental liquid and vapor density of DMSO, 1100 g L^{-1} and 3.43 g L^{-1}, respectively *(both at standard conditions)*, we obtained $\Delta V =$ 22.71 L mol^{-1}, and therefore $p\Delta V = 2.3\,kJ\,mol^{-1}$, which needs to be added to the internal energies of vaporization.

The results are presented in Table 6. We performed the computational protocol with both the original DMSO force field (OPLS–AA) and our optimized force field (BILFF) and compare the obtained values to the experimental reference value. While the resulting enthalpy of vaporization based on OPLS–AA is 3.4% too small, the value based on BILFF is 2.4% too large. We conclude that the resulting enthalpies of vaporization for pure DMSO based on both force fields are reasonable and very well within the expected range, and that the result based on BILFF is slightly better in comparison to experiment.

Conclusion

In this article, we present the extension of the all-atom force field for *B*io-Polymers in *I*onic *L*iquids (short: BILFF) to the co-solvent DMSO, which significantly increases the solubility of cellulose in ionic liquids such as [EMIm][OAc] (Anokhina et al. 2017, Mohan et al. 2016, Tomimatsu et al. 2019, Xu et al. 2013, Yang et al. 2019b). Previously, we published optimized force field parameters for the ionic liquids 1-ethyl-3-methylimidazolium acetate ([EMIm][OAc]) (Roos and Brehm 2021), 1-ethyl-3-methyl-1,2,3-triazolium acetate ([EMTr][OAc]), 1-ethyl-3-methyl-1,2,3-triazolium benzoate ([EMTr][OBz]), and 1-ethyl-3-methylimidazolium benzoate ([EMIm][OBz]) (Roos et al. 2023a) and cellulose (Roos et al. 2023b).

The force field was developed for an accurate reproduction of the directed interactions in DMSO/[EMIm][OAc] in the presence and absence of water with a special focus on the hydrogen bonds. For this purpose, the radial distribution functions, the

distance–angle distribution functions, and the density and statistical frequency of occurring bond lengths, angles, and dihedral angles were analyzed and compared with the results of reference AIMD simulations as well as experimental density measurements. Based on this comparison, the force field parameters were iteratively adjusted until the deviations between the results from the force field MD and AIMD simulation were minimized. The force field was validated by experimental data on density, self-diffusion coefficients, enthalpy of vaporization, thermal expansion coefficient and compressibility of the different systems, showing excellent or at least reasonable agreement with literature data. Furthermore, an applicability of our optimized force field parameters at higher temperatures was shown based on a comparison with reference AIMD simulations.

The simulation results show that DMSO forms a solvation shell around $[EMIm]^+$ and thus shields it from $[OAc]^-$. This is consistent with the prevailing theory in the literature that $[OAc]^-$ is more freely available for interaction with cellulose due to the DMSO shielding, thus increasing cellulose solubility (Mohan et al. 2016, Tomimatsu et al. 2019, Xu and Zhang 2015). In the aqueous system, the underlying hydrogen bond network is more complicated, as water is also a strong hydrogen bond donor for DMSO. The lifetime of the cation–anion hydrogen bond in DMSO/IL/water is even increased. Due to the complexity of the underlying interaction network, no trivial answer to this apparent contradiction can be given here.

The diffusion rate is increased by DMSO compared to the pure IL, which is also consistent with the literature mechanism (Le et al. 2014, Tomimatsu et al. 2019) and is considered to be another reason for the increased cellulose solubility in DMSO/IL.

Author contributions ER: Data curation, Data analysis, Visualization of the results, Writing of the original manuscript draft. CG: Data analysis, Writing of text passages of the original manuscript draft, MB: Choice of computational methods, Supervision. DS: Supervision, Conceptualization. All authors contributed to the analysis and interpretation of the results, as well as further review iterations of the manuscript.

Data Availability Statement The corresponding author [MB] can be contacted for available data supporting the findings of this study.

Declarations

Conflicts of interest There are no conflicts of interest to declare.

Ethics approval Not applicable.

Consent for publication Not applicable.

Competing interests The authors declare no competing interests.

References

Abeer MM, Amin M, Iqbal MC, Martin C (2014) A review of bacterial cellulose-based drug delivery systems: their biochemistry, current approaches and future prospects. J Pharm Pharmacol 66(8):1047–1061. https://doi.org/10.1111/jphp.12234

Andersen HC (1983) Rattle: a "velocity" version of the shake algorithm for molecular dynamics calculations. J Comput Phys 52(1):24–34. https://doi.org/10.1016/0021-9991(83)90014-1

Anokhina TS, Pleshivtseva TS, Ignatenko VY, Antonov SV, Volkov AV (2017) Fabrication of composite nanofiltration membranes from cellulose solutions in an [emim]oac–dmso mixture. Pet Chem 57(6):477–482. https://doi.org/10.1134/S0965544117060020

Azimi B, Maleki H, Gigante V, Bagherzadeh R, Mezzetta A, Milazzo M, Guazzelli L, Cinelli P, Lazzeri A, Danti S (2022) Cellulose-based fiber spinning processes using ionic liquids. Cellulose 29(6):3079–3129. https://doi.org/10.1007/s10570-022-04473-1

Becke A (1988) Density-functional exchange-energy approximation with correct asymptotic behavior. Phys Rev A 38:3098–3100. https://doi.org/10.1103/PhysRevA.38.3098

Berendsen HJC, Postma JPM, van Gunsteren WF, DiNola A, Haak JR (1984) Molecular dynamics with coupling to an external bath. J Chem Phys 81(8):3684–3690. https://doi.org/10.1063/1.448118

Bordat P, Sacristan J, Reith D, Girard S, Glättli A, Müller-Plathe F (2003) An improved dimethyl sulfoxide force field for molecular dynamics simulations. Chem Phys Lett 374(3–4):201–205. https://doi.org/10.1016/S0009-2614(03)00550-5

Brehm M, Kirchner B (2011) Travis - a free analyzer and visualizer for monte carlo and molecular dynamics trajectories. J Chem Inf Model 51(8):2007–2023. https://doi.org/10.1021/ci200217w

Brehm M, Sebastiani D (2018) Simulating structure and dynamics in small droplets of 1-ethyl-3-methylimidazolium acetate. J Chem Phys 148(19):193802. https://doi.org/10.1063/1.5010342

Brehm M, Pulst M, Kressler J, Sebastiani D (2019) Triazolium-based ionic liquids: a novel class of cellulose solvents. J Phys Chem B 123(18):3994–4003. https://doi.org/10.1021/acs.jpcb.8b12082

Brehm M, Radicke J, Pulst M, Shaabani F, Sebastiani D, Kressler J (2020) Dissolving cellulose in 1,2,3-triazolium- and imidazolium-based ionic liquids with aromatic anions. Molecules 25(15):3539–3559. https://doi.org/10.3390/molecules25153539

Brehm M, Thomas M, Gehrke S, Kirchner B (2020) Travis-a free analyzer for trajectories from molecular simulation. J Chem Phys 152(16):164105. https://doi.org/10.1063/5.0005078

Ciocirlan O, Iulian O (2012) Properties of pure 1-butyl-2,3-dimethylimidazolium tetrafluoroborate ionic liquid and its binary mixtures with dimethyl sulfoxide and acetonitrile. J Chem Eng Data 57(11):3142–3148. https://doi.org/10.1021/je3007474

Cornell WD, Cieplak P, Bayly CI, Gould IR, Merz KM, Ferguson DM, Spellmeyer DC, Fox T, Caldwell JW, Kollman PA (1995) A second generation force field for the simulation of proteins, nucleic acids, and organic molecules. J Am Chem Soc 117(19):5179–5197. https://doi.org/10.1021/ja00124a002

Cowie JMG, Toporowski PM (1961) Association in the binary liquid system dimethyl sulfoxide – water. Can J Chem 39(11):2240–2243. https://doi.org/10.1139/v61-296

Douglas TB (1948) Vapor pressure of methyl sulfoxide from 20 to 50°. calculation of the heat of vaporization. J Am Chem Soc 70(6):2001–2002. https://doi.org/10.1021/ja01186a005

Dünweg B, Paul W (1991) Brownian dynamics simulations without gaussian random numbers. Int J Mod Phys C 02(03):817–827. https://doi.org/10.1142/S0129183191001037

Egorov GI, Makarov DM, Kolker AM (2010) Densities and volumetric properties of ethylene glycol + dimethylsulfoxide mixtures at temperatures of (278.15 to 323.15) k and pressures of (0.1 to 100) mpa. J Chem Eng Data 55(9):3481–3488. https://doi.org/10.1021/je100089s

Fang S, Lyu X, Tong T, Lim AI, Li T, Bao J, Hu YH (2023) Turning dead leaves into an active multifunctional material as evaporator, photocatalyst, and bioplastic. Nat Commun 14(1):1203. https://doi.org/10.1038/s41467-023-36783-8

Fox T, Kollman PA (1998) Application of the resp methodology in the parametrization of organic solvents. J Phys Chem B 102(41):8070–8079. https://doi.org/10.1021/jp9717655

Froschauer C, Hummel M, Iakovlev M, Roselli A, Schottenberger H, Sixta H (2013) Separation of hemicellulose and cellulose from wood pulp by means of ionic liquid/cosolvent systems. Biomacromol 14(6):1741–1750. https://doi.org/10.1021/bm400106h

Geerke DP, Oostenbrink C, van der Vegt NFA, van Gunsteren WF (2004) An effective force field for molecular dynamics simulations of dimethyl sulfoxide and dimethyl sulfoxide−water mixtures. J Phys Chem B 108(4):1436–1445. https://doi.org/10.1021/jp035034i

Gehrke S, von Domaros M, Clark R, Hollóczki O, Brehm M, Welton T, Luzar A, Kirchner B (2018) Structure and lifetimes in ionic liquids and their mixtures. Faraday Discuss 206:219–245. https://doi.org/10.1039/C7FD00166E

Goedecker S, Teter M, Hutter J (1996) Separable dual-space gaussian pseudopotentials. Phys Rev B 54:1703–1710. https://doi.org/10.1103/PhysRevB.54.1703

Grace Development Team (1996) see http://plasma-gate.weizmann.ac.il/grace

Green SM, Ries ME, Moffat J, Budtova T (2017) Nmr and rheological study of anion size influence on the properties of two imidazolium-based ionic liquids. Sci Rep 7(1):8968. https://doi.org/10.1038/s41598-017-09509-2

Grimme S, Antony J, Ehrlich S, Krieg H (2010) A consistent and accurate ab initio parametrization of density functional dispersion correction (dft-d) for the 94 elements h-pu. J Chem Phys 132(15):154104. https://doi.org/10.1063/1.3382344

Grimme S, Ehrlich S, Goerigk L (2011) Effect of the damping function in dispersion corrected density functional theory. J Comput Chem 32(7):1456–1465. https://doi.org/10.1002/jcc.21759

Hall CA, Le KA, Rudaz C, Radhi A, Lovell CS, Damion RA, Budtova T, Ries ME (2012) Macroscopic and microscopic study of 1-ethyl-3-methyl-imidazolium acetate-water mixtures. J Phys Chem B 116(42):12810–12818. https://doi.org/10.1021/jp306829c

Hartwigsen C, Goedecker S, Hutter J (1998) Relativistic separable dual-space gaussian pseudopotentials from h to rn. Phys Rev B 58:3641–3662. https://doi.org/10.1103/PhysRevB.58.3641

Himmel ME, Ding SY, Johnson DK, Adney WS, Nimlos MR, Brady JW, Foust TD (2007) Biomass recalcitrance: engineering plants and enzymes for biofuels production. Science 315(5813):804–807. https://doi.org/10.1126/science.1137016

Hohenberg P, Kohn W (1964) Inhomogeneous electron gas. Phys Rev B 136:864. https://doi.org/10.1103/PhysRev.136.B864

Holz M, Heil SR, Sacco A (2000) Temperature-dependent self-diffusion coefficients of water and six selected molecular liquids for calibration in accurate 1h nmr pfg measurements. Phys Chem Chem Phys 2(20):4740–4742. https://doi.org/10.1039/B005319H

Horn HW, Swope WC, Pitera JW, Madura JD, Dick TJ, Hura GL, Head-Gordon T (2004) Development of an improved four-site water model for biomolecular simulations: Tip4p-ew. J Chem Phys 120(20):9665–9678. https://doi.org/10.1063/1.1683075

Humphrey W, Dalke A, Schulten K (1996) Vmd: visual molecular dynamics. J Mol Graph 14(1):33–38. https://doi.org/10.1016/0263-7855(96)00018-5

Hutter J, Iannuzzi M, Schiffmann F, VandeVondele J (2014) Cp2k: atomistic simulations of condensed matter systems. Comput Mol Sci 4(1):15–25. https://doi.org/10.1002/wcms.1159

J Stone (1998) Msc thesis. Computer Science Department, University of Missouri-Rolla

Jorgensen WL, Maxwell DS, Tirado-Rives J (1996) Development and testing of the opls all-atom force field on conformational energetics and properties of organic liquids. J Am Chem Soc 118(45):11225–11236. https://doi.org/10.1021/ja9621760

Kirchner B, Reiher M (2002) The secret of dimethyl sulfoxide-water mixtures. a quantum chemical study of 1dmso-n water clusters. J Am Chem Soc 124(21):6206–6215. https://doi.org/10.1021/ja017703g

Klemm D, Heublein B, Fink HP, Bohn A (2005) Cellulose: fascinating biopolymer and sustainable raw material. Angew Chem 44(22):3358–3393. https://doi.org/10.1002/anie.200460587

Kohagen M, Brehm M, Lingscheid Y, Giernoth R, Sangoro J, Kremer F, Naumov S, Iacob C, Kärger J, Valiullin R, Kirchner B (2011) How hydrogen bonds influence the mobility of imidazolium-based ionic liquids. a combined theoretical and experimental study of 1-n-butyl-3-methylimidazolium bromide. J Phys Chem B 115(51):15280–15288. https://doi.org/10.1021/jp206974h

Kohn W, Sham L (1965) Self-consistent equations including exchange and correlation effects. Phys Rev 140:1133. https://doi.org/10.1103/PhysRev.140.A1133

Kühne TD, Iannuzzi M, Del Ben M, Rybkin VV, Seewald P, Stein F, Laino T, Khaliullin RZ, Schütt O, Schiffmann F, Golze D, Wilhelm J, Chulkov S, Bani-Hashemian MH, Weber V, Borštnik U, Taillefumier M, Jakobovits AS, Lazzaro A, Pabst H, Müller T, Schade R, Guidon M, Andermatt S, Holmberg N, Schenter GK, Hehn A, Bussy A, Belleflamme F, Tabacchi G, Glöß A, Lass M, Bethune I, Mundy CJ, Plessl C, Watkins M, VandeVondele J, Krack M, Hutter J (2020) Cp2k: An electronic structure and molecular dynamics software package - quickstep: efficient and accurate electronic structure calculations. J Chem Phys 152(19):194103. https://doi.org/10.1063/5.0007045

Le KA, Sescousse R, Budtova T (2012) Influence of water on cellulose-emimac solution properties: a viscometric study. Cellulose 19(1):45–54. https://doi.org/10.1007/s10570-011-9610-3

Le KA, Rudaz C, Budtova T (2014) Phase diagram, solubility limit and hydrodynamic properties of cellulose in binary solvents with ionic liquid. Carbohydr Polym 105:237–243. https://doi.org/10.1016/j.carbpol.2014.01.085

Lee C, Yang W, Parr R (1988) Development of the colle-salvetti correlation-energy formula into a functional of the electron density. Phys Rev B 37:785–789. https://doi.org/10.1103/PhysRevB.37.785

Li C, Tanjore D, He W, Wong J, Gardner JL, Sale KL, Simmons BA, Singh S (2013) Scale-up and evaluation of high solid ionic liquid pretreatment and enzymatic hydrolysis of switchgrass. Biotechnol Biofuels 6(1):154. https://doi.org/10.1186/1754-6834-6-154

Liu H, Mueller-Plathe F, van Gunsteren WF (1995) A force field for liquid dimethyl sulfoxide and physical properties of liquid dimethyl sulfoxide calculated using molecular dynamics simulation. J Am Chem Soc 117(15):4363–4366. https://doi.org/10.1021/ja00120a018

Lü P, Zhao G, Zhang X, Yin J, Bao J (2016) Measurement and prediction on the surface properties of dimethyl sulfoxide/water mixtures. Chem Res Chin Univ 32(1):100–105. https://doi.org/10.1007/s40242-016-5297-1

Malberg F, Brehm M, Hollóczki O, Pensado AS, Kirchner B (2013) Understanding the evaporation of ionic liquids using the example of 1-ethyl-3-methylimidazolium ethylsulfate. Phys Chem Chem Phys 15(42):18424–18436. https://doi.org/10.1039/C3CP52966E

Manna B, Ghosh A (2019) Dissolution of cellulose in ionic liquid and water mixtures as revealed by molecular dynamics simulations. J Biomol Struct Dyn 37(15):3987–4005. https://doi.org/10.1080/07391102.2018.1533496

Martínez L, Andrade R, Birgin EG, Martínez JM (2009) Packmol: a package for building initial configurations for molecular dynamics simulations. J Comput Chem 30(13):2157–2164. https://doi.org/10.1002/jcc.21224

Martyna G, Klein M, Tuckerman M (1992) Nosé-Hoover chains: The canonical ensemble via continuous dynamics. J Chem Phys 97:2535–2643. https://doi.org/10.1063/1.463940

Mohan M, Banerjee T, Goud VV (2016) Effect of protic and aprotic solvents on the mechanism of cellulose dissolution in ionic liquids: a combined molecular dynamics and experimental insight. ChemistrySelect 1(15):4823–4832. https://doi.org/10.1002/slct.201601094

Nanda S, Patra BR, Patel R, Bakos J, Dalai AK (2022) Innovations in applications and prospects of bioplastics and biopolymers: a review. Environ Chem Lett 20(1):379–395. https://doi.org/10.1007/s10311-021-01334-4

Nisa LdP, Mugang M, Bermejo MD, Segovia Puras JJ, Pérez E (2019) Density and melting points for the binary mixtures dimethyl sulfoxide (dmso) + 1-ethyl-3-methylimidazolium acetate and dmso + choline acetate. J Chem Eng Data 64(7):2923–2928. https://doi.org/10.1021/acs.jced.8b01048

Nose S (1984a) A molecular dynamics method for simulations in the canonical ensemble. Mol Phys 52:255–268. https://doi.org/10.1080/00268978400101201

Nose S (1984b) A unified formulation of the constant temperature molecular dynamics methods. J Chem Phys 81:511–519. https://doi.org/10.1063/1.447334

Olsson C, Westman G (2013) Direct dissolution of cellulose: Background, means and applications. Cellulose-Fundamental Aspects, pp 143–178. https://doi.org/10.5772/52144

Packer KJ, Tomlinson DJ (1971) Nuclear spin relaxation and self-diffusion in the binary system, dimethylsulphoxide (dmso)+water. Trans Faraday Soc 67:1302–1314. https://doi.org/10.1039/TF9716701302

Paiva TG, Zanatta M, Cabrita EJ, Bernardes CE, Corvo MC (2022) Dmso/il solvent systems for cellulose dissolution: binary or ternary mixtures? J Mol Liq 345:117810. https://doi.org/10.1016/j.molliq.2021.117810

Paknejad A, Mohammadkhani R, Zarei H (2019) Experimental high-temperature, high-pressure density measurement and perturbed-chain statistical associating fluid theory modeling of dimethyl sulfoxide, isoamyl acetate, and benzyl alcohol. J Chem Eng Data 64(12):5174–5184. https://doi.org/10.1021/acs.jced.9b00396

Payne CM, Knott BC, Mayes HB, Hansson H, Himmel ME, Sandgren M, Ståhlberg J, Beckham GT (2015) Fungal cellulases. Chem Rev 115(3):1308–1448. https://doi.org/10.1021/cr500351c

Plimpton S (1995) Fast parallel algorithms for short-range molecular dynamics. J Comp Phys 117:1–19. https://doi.org/10.1006/jcph.1995.1039

Ponder JW, Case DA (2003) Force fields for protein simulations. Adv Protein Chem 66:27–85. https://doi.org/10.1016/S0065-3233(03)66002-X

Radhi A, Le KA, Ries ME, Budtova T (2015) Macroscopic and microscopic study of 1-ethyl-3-methyl-imidazolium acetate-dmso mixtures. J Phys Chem B 119(4):1633–1640. https://doi.org/10.1021/jp5112108

Rapaport DC (1983) Hydrogen bonds in water. Mol Phys 50(5):1151–1162. https://doi.org/10.1080/00268978300102931

Roos E, Brehm M (2021) A force field for bio-polymers in ionic liquids (bilff) - part 1: Emimoac/water mixtures. PCCP 23(2):1242–1253. https://doi.org/10.1039/d0cp04537c

Roos E, Sebastiani D, Brehm M (2023b) A force field for bio-polymers in ionic liquids (bilff) - part 2: cellulose in emimoac/water mixtures. PCCP. https://doi.org/10.1039/D2CP05636D

Roos E, Sebastiani D, Brehm M (2023a) Bilff: All-atom force field for modeling triazolium- and benzoate-based ionic liquids. Molecules 28(22). https://doi.org/10.3390/molecules28227592

Ryckaert JP, Ciccotti G, Berendsen HJ (1977) Numerical integration of the cartesian equations of motion of a system with constraints: molecular dynamics of n-alkanes. J Comput Phys 23(3):327–341. https://doi.org/10.1016/0021-9991(77)90098-5

Sambasivarao SV, Acevedo O (2009) Development of opls-aa force field parameters for 68 unique ionic liquids. J Chem Theory Comput 5(4):1038–1050. https://doi.org/10.1021/ct900009a

Schneider T, Stoll E (1978) Molecular-dynamics study of a three-dimensional one-component model for distortive phase transitions. Phys Rev B 17(3):1302–1322. https://doi.org/10.1103/PhysRevB.17.1302

Smith DGA, Burns LA, Patkowski K, Sherrill CD (2016) Revised damping parameters for the d3 dispersion correction to density functional theory. J Phys Chem Lett 7(12):2197–2203. https://doi.org/10.1021/acs.jpclett.6b00780

Strader ML, Feller SE (2002) A flexible all-atom model of dimethyl sulfoxide for molecular dynamics simulations. J Phys Chem A 106(6):1074–1080. https://doi.org/10.1021/jp013658n

Sun Y, Cheng J (2002) Hydrolysis of lignocellulosic materials for ethanol production: a review. Bioresour Technol 83(1):1–11. https://doi.org/10.1016/S0960-8524(01)00212-7

Swatloski RP, Spear SK, Holbrey JD, Rogers RD (2002) Dissolution of cellulose with ionic liquids. J Am Chem Soc 124(18):4974–4975. https://doi.org/10.1021/ja025790m

The CP2K developers group (2017) Cp2k is freely available from http://www.cp2k.org/

Thomas B, Raj MC, B AK, H RM, Joy J, Moores A, Drisko GL, Sanchez C (2018) Nanocellulose, a versatile green platform: From biosources to materials and their applications. Chem Rev 118(24):11575–11625. https://doi.org/10.1021/acs.chemrev.7b00627

Tomimatsu Y, Suetsugu H, Yoshimura Y, Shimizu A (2019) The solubility of cellulose in binary mixtures of ionic liquids and dimethyl sulfoxide: influence of the anion. J Mol Liq 279:120–126. https://doi.org/10.1016/j.molliq.2019.01.093

VandeVondele J, Hutter J (2003) An efficient orbital transformation method for electronic structure calculations. J Chem Phys 118(10):4365–4369. https://doi.org/10.1063/1.1543154

VandeVondele J, Hutter J (2007) Gaussian basis sets for accurate calculations on molecular systems in gas and condensed phases. J Chem Phys 127:114105. https://doi.org/10.1063/1.2770708

VandeVondele J, Krack M, Mohamed F, Parrinello M, Chassaing T, Hutter J (2005) Quickstep: fast and accurate density functional calculations using a mixed gaussian and plane waves approach. Comput Phys Commun 167(2):103–128. https://doi.org/10.1016/j.cpc.2004.12.014

Wanichapichart P, Taweepreeda W, Nawae S, Choomgan P, Yasenchak D (2012) Chain scission and anti fungal effect of electron beam on cellulose membrane. Radiat Phys Chem 81(8):949–953. https://doi.org/10.1016/j.radphyschem.2012.02.035

Wolfram Research, Inc (2010) Mathematica, version 8.0, champaign, il

Xu A, Zhang Y (2015) Insight into dissolution mechanism of cellulose in [c4mim][ch3coo]/dmso solvent by 13c nmr spectra. J Mol Struct 1088:101–104. https://doi.org/10.1016/j.molstruc.2015.02.031

Xu A, Zhang Y, Zhao Y, Wang J (2013) Cellulose dissolution at ambient temperature: role of preferential solvation of cations of ionic liquids by a cosolvent. Carbohydr Polym 92(1):540–544. https://doi.org/10.1016/j.carbpol.2012.09.028

Yang F, Wang X, Chen Q, Tan H (2019) Improvement of the properties of 1-ethyl-3-methylimidazolium acetate using organic solvents for biofuel process. J Mol Liq 284:82–91. https://doi.org/10.1016/j.molliq.2019.03.144

Yang M, Zhao W, Wang S, Yu C, Singh S, Simmons B, Cheng G (2019) Dimethyl sulfoxide assisted dissolution of cellulose in 1-ethyl-3-methylimidazoium acetate: small angle neutron scattering and rheological studies. Cellulose 26(4):2243–2253. https://doi.org/10.1007/s10570-018-2218-0

Yousefi Shivyari N, Tajvidi M, Bousfield DW, Gardner DJ (2016) Production and characterization of laminates of paper and cellulose nanofibrils. ACS 8(38):25520–25528. https://doi.org/10.1021/acsami.6b07655

Zhang X, Cheng Y, You J, Zhang J, Yin C, Zhang J (2022) Ultralong phosphorescence cellulose with excellent anti-bacterial, water-resistant and ease-to-process performance. Nat Commun 13(1):1117. https://doi.org/10.1038/s41467-022-28759-x